Journal of Colloid and Interface Science 444 (2015) 87–96

Contents lists available at ScienceDirect

Journal of Colloid and Interface Science

www.elsevier.com/locate/jcis

A hydrothermal peroxo method for preparation of highly crystalline silica–titania photocatalysts

Igor Krivtsov [a,b,*], Marina Ilkaeva [a,c], Viacheslav Avdin [b,c], Sergei Khainakov [a], Jose R. Garcìa [a], Salvador Ordòñez [d], Eva Dìaz [d], Laura Faba [d]

[a] Department of Organic and Inorganic Chemistry, University of Oviedo, Julian Claveria s/n, Oviedo 33006, Spain
[b] Nanotechnology Education and Research Center, South Ural State University, Lenina Ave. 76, Chelyabinsk 454080, Russia
[c] Department of Chemistry, South Ural State University, Lenina Ave. 76, Chelyabinsk 454080, Russia
[d] Department of Chemical and Environmental Engineering, University of Oviedo, Julián Clavería s/n, Oviedo 33006, Spain

GRAPHICAL ABSTRACT

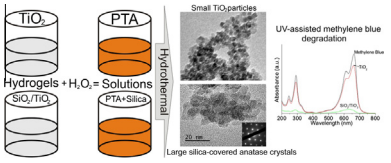

ARTICLE INFO

Article history:
Received 17 September 2014
Accepted 8 December 2014
Available online 26 December 2014

Keywords:
Peroxo complex
Peroxo titanic acid
Crystallinity
Anatase
SiO_2–TiO_2

ABSTRACT

A new completely inorganic method of preparation of silica–titania photocatalyst has been described. It has been established that the addition of silica promotes crystallinity of TiO_2 anatase phase. Relative crystallinity and TiO_2 crystal size in the silica–titania particles increase with the silica content until SiO_2/TiO_2 molar ratio of 0.9, but at higher molar ratios they start to decrease. The single-source precursor containing peroxo titanic (PTA) and silicic acids has been proved to be responsible for high crystallinity of TiO_2 encapsulated into amorphous silica. It has been proposed that peroxo groups enhance rapid formation of crystalline titania seeds, while silica controls their growth. It has been concluded from the TEM that the most morphologically uniform anatase crystallites covered with SiO_2 particles are prepared at SiO_2/TiO_2 molar ratio of 0.4. This sample, according to ^{29}Si NMR, also shows the high content of hydroxylated silica Q^3 and Q^2 groups, and it is the most photocatalytically active in UV-assisted decomposition of methylene blue among the tested materials. It has been determined that the increase in the amount of the condensed Q^4 silica in the mixed oxides leads to the decrease in photocatalytic performance of the material, despite its better crystallinity. High crystallinity, low degree of incorporation of Ti atoms in SiO_2 in the mixed oxide and adsorption of methylene blue in the vicinity of photoactive sites on the hydroxylated silica have been considered as the main factors determining the high degradation degree of methylene blue in the presence of silica–titania.

1. Introduction

Titania is an excellent photocatalyst, whose applications, properties, structural and morphological features are well known and summarized in the number of comprehensive reviews [1–12]. However, the search for the procedures able to ensure TiO_2 with better qualities for photocatalytic applications is still a key issue. Recently, the industry and researchers have turned towards

* Corresponding author at: Julian Claveria 8, Oviedo 33006, Spain.
E-mail addresses: zapasoul@gmail.com, uo247495@uniovi.es (I. Krivtsov), uo247496@uniovi.es, mylegenda@gmail.com (M. Ilkaeva), avdinvv@susu.ac.ru (V. Avdin), khaynakovsergiy@uniovi.es (S. Khainakov), jrgm@uniovi.es (J.R. Garcìa), sordonez@uniovi.es (S. Ordòñez), diazfeva@uniovi.es (E. Dìaz), fabalaura@uniovi.es (L. Faba).

http://dx.doi.org/10.1016/j.jcis.2014.12.044
0021-9797/

"green" and more economically reasonable technologies. In the field of oxide materials it means that alternative ways for preparation of oxides have to be found, instead of the most widespread alkoxide-based procedures. As a consequence, several reviews on the utilization of peroxo complexes of transition metals [13] and titanium in particular [14,15] have been published. Water-soluble peroxo complexes of transition metals are considered as "green" and inexpensive sources of nanostructured metal oxide catalysts, since application of toxic alkoxides or solvents and organic ligands is not needed. Aqueous titanium peroxo complexes can exist in the wide range of pH values in low-nuclear forms, which allows controlling their phase composition, obtaining 100% pure anatase, rutile or brookite phases [16,17]. Also the peroxo route of TiO_2 synthesis is found to be flexible enough to control shape, sizes and preferential orientation of titania crystals [18–22]. In spite of the fact that this method is inexpensive and allows controlling various titania properties, it has seldom been applied for preparation of mixed silica–titania oxides, which could posses improved photocatalytic properties. The information on application of the peroxo route to SiO_2/TiO_2 synthesis is scarce; being limited to the thin film preparation or impregnation of the preformed silica colloidal particles with titanium peroxo complex [23]. However, modification of titanium oxide with silica is a widespread method [24] aiming to increase the thermal stability of its most photocatalytically active polymorph anatase [25], tune the sizes of its crystals [26], increase the surface area [27], improve adsorption properties [26], and introduce mesoporosity to the mixed SiO_2/TiO_2 material [28]. This modification can be achieved by preparation of a highly homogeneous mixed oxide [29], by covering the preformed crystalline titania particles with silica layer [30], or making it otherwise, crystallizing anatase on the surface of colloidal SiO_2 spheres [31]. Sol–gel technique is found to be the most applicable to the abovementioned purposes. Hydrothermal method, on the other hand, is less common for SiO_2/TiO_2 particles preparation; only several reports on the application of this procedure were published [26,32,33].

Besides the obvious advantages that silica contributes to the mixed silica–titania, it also gives a significant drawback. As a rule, silica in the mixed oxide causes formation of defects and suppresses the growth of TiO_2 crystals [29,34–37]. However, it is known that high crystallinity is an important feature, as the electron pairs recombination takes place on the crystalline defects; this reduces the activity of the photocatalyst [38–40]. In spite of a common view attributing the enhancement of the photocatalytic activity to the decrease of the anatase particles [41,42], it might be supposed that the increase of the TiO_2 crystal sizes could favor lowering recombination rate and improve its catalytic properties. The benefit that silica introduces to the mixed oxide is difficult to combine with high crystallinity of TiO_2. In order to achieve reasonable crystallinity in silica–titania, heat treatment at temperatures up to 800 °C is applied [25]. However, we have not found any reports on the preparation of highly crystalline SiO_2/TiO_2 oxides under mild conditions. In the present study we describe a new method of silica–titania particles synthesis and the unusual effect that silica has on the crystallization of TiO_2 under hydrothermal conditions, as it promotes titania crystallinity rather than suppresses it. The test of the prepared materials in the photocatalytic degradation of methylene blue dye shows their high activity.

2. Experimental

2.1. Chemicals

Non-volatile and stable under ambient conditions titanium oxysulfate hydrate ($TiOSO_4 \cdot H_2O$), containing not more than 17 wt% of sulfuric acid, and 27 wt% solution of sodium silicate ($Na_2Si_3O_7$) in water were purchased from Aldrich and used as the sources of titania and silica, respectively. Sodium hydroxide (Prolabo, 99% purity) was used as precipitation agent, 20% ammonia solution in water (Prolabo) and nitric acid (Prolabo) were applied for pH correction. Hydrogen peroxide 30 wt% solution was obtained from Aldrich. Methylene blue was of analytical grade.

2.2. Synthesis

On the first stage of the synthesis, 50 mL of sodium silicate solution with concentrations: 0.0, 0.025, 0.05, 0.1, 0.14 and 0.18 mol/L was added to 50 mL of 0.1 M solution of $TiOSO_4$. The samples were designated as 0TS, 0.1TS, 0.4TS, 0.9TS, 1.3TS, and 1.6TS (where the numbers indicate SiO_2/TiO_2 molar ratio in the synthesized samples, determined by elemental analysis). Then the mixtures were hydrolyzed with 1.5 M solution of sodium hydroxide, the addition of NaOH ended when the pH value reached 3.2 (4.0 for 0TS and 0.1TS). The gel-like precipitates obtained after alkali addition were centrifuged at 3000 r.p.m. and thoroughly washed with deionized water eight times, until the negative reaction on sulfate ions. On the next stage, 0.5 mL of 3 M ammonia was added to the precipitate following by ultrasonication in 50 mL of distilled water. Then to the dispersed precipitates 4 mL of H_2O_2 solution was added and the pH of the reaction mixtures was adjusted to 7.0 by the addition of ammonia solution in order to obtain water-soluble titanium peroxo complexes. Soon, the clear transparent yellow solutions of titanium peroxo complex and silicic acid were formed. The findings concerning dissolution of silica–titania hydrogel in hydrogen peroxide were described elsewhere [43,44]. The pH of the solution was adjusted to 7.0 with ammonia. After that, 3 M nitric acid was dropwise introduced to the solution until pH reached the value of 2.0. It is worth mentioning that after the addition of acid all solutions stayed clear with an exception of the samples 0TS and 0.1TS, where the formation of sol was observed. Then the volume of the prepared mixtures was adjusted to 80 mL by deionized water and they were transferred to Teflon-lined stainless steel autoclaves having total volume of 140 mL for hydrothermal treatment. Hydrothermal treatment was carried out under autogenic pressure at 180 °C during 48 h. In order to establish the role of the precursor, silica–titania materials with the equimolar SiO_2/TiO_2 composition in the reaction mixture, were also synthesized under conditions of pH not being controlled by ammonia and nitric acid addition (PTA–SiO_2), by hydrothermal treatment of the gel in the absence of hydrogen peroxide after ammonia and nitric acid were added (GelTS), and using separately prepared titanium peroxo complex and sodium silicate solution (NH_3PT–SiO_2). When the treatment was over, the precipitates were isolated by centrifugation at 3000 r.p.m., washed with deionized water eight times and dried at 60 °C for 24 h. In order to eliminate adsorbed water, the samples were calcined in static air at 400 °C for 2 h, but a part of each sample was left as-synthesized as well.

2.3. Characterization

X-ray diffraction patterns were registered using Rigaku Ultima IV diffractometer, operating at Cu K_α radiation ($\lambda = 0.15418$ nm) at voltage of 30 kV with a help of high-speed DTEX detector. Scherrer equation was applied to estimate the mean crystallite size of TiO_2 by the (1 0 1) reflection, the uncertainty of the estimation is near 5%. Unit cell parameters for anatase crystals were refined using GSAS software [45]. Relative crystallinity was estimated from the ratio of anatase peak intensity of (1 0 1) reflection to that of the 0TS sample calcined at 400 °C [46,47]. Scanning electron microscope Jeol JSM 7001F with Oxford Instruments EDS-attachment was used to investigate morphology and to determine elemental

composition of the prepared materials. The samples were preliminary coated by magnetron sputtering with approximately 3 nm thick gold layer Transmission electron microscopy (TEM) images were carried out using a Jeol 200 EX-II and a Jeol JEM 2100F, the elemental composition of the particles was obtained by EDS-attachment to the microscope. The samples were dispersed in ethanol and then few drops of the suspension were put on a copper grid prior to investigation Infrared spectra were collected from the samples powdered with KBr and pressed in pellets, by Bruker Tensor 27 FTIR spectrometer. Diffusive-reflectance ultraviolet–visible light (DR UV) spectra were registered from the powdered samples supported on barium sulfate pellets in a Shimadzu UV-2700 UV–vis spectrophotometer with an integrated sphere attachment. Band gap energy was determined from the DR UV spectra by Kubelka-Munk method. Micromeritics ASAP 2020 was used to obtain adsorption–desorption isotherms of N_2 at 77 K. The surface area and pore volume were calculated from the low-temperature nitrogen adsorption data using BET and BJH approaches. Prior to the experiment the samples were degassed under vacuum at 400 °C for 4 h. The solid state ^{29}Si MAS NMR and ^{1}H–^{29}Si cross-polarization MAS NMR (CPMAS) measurements were recorded on a Bruker Avance III 400WB spectrometer at 79.49 MHz for ^{29}Si. The experiment was done at ambient temperature with a sample spinning rate of 4500 Hz (45° pulse width of 2.5 μs). For calibration of the ^{29}Si signal position Q8M8 reference material was used. For the NMR MAS measurement a pulse delay of 180 s was chosen, and the number of scans was 3000. For the CPMAS NMR experiment a pulse delay was 5 s, and the number of scans was 1000. The surface composition and binding energy of Si, Ti and O in pure titania and mixed oxides were measured by X-ray Photoelectron Spectroscopy (XPS), using a SPECS system equipped with a Hemispherical Phoibos detector operating in a constant pass energy, using Mg Kα radiation ($h \cdot \upsilon$ = 1253.6 eV). The content of sulfur was determined using CHNS Elementar vario MACRO analyzer.

2.4. Photocatalytic activity test

Synthesized silica–titania materials were tested in the aqueous-phase photocatalytic degradation of methylene blue (MB) in a stirred batch reactor. For the experiment 25 mg of each sample calcined in air at 400 °C for 2 h was taken into a quartz reactor. Then 50 mL of the aqueous solution of MB with concentration 20 mg L^{-1} was added to the catalyst. Firstly, the adsorption of MB by the catalyst was determined, for this the suspension was magnetically stirred in the dark until it reached the adsorption equilibrium (for the Degussa P25, 0TS, 0.1TS, 0.4TS and 0.9TS the equilibrium was reached after 30 min, while longer time was needed to the 1.3TS and 1.6TS samples), then the concentration of MB was photometrically determined by the absorbance at 664 nm using Shimadzu UV-2700 spectrophotometer. After the dark experiment the suspension was exposed to ultraviolet irradiation. The source of UV-light was the Osram high-pressure mercury 125 W lamp. It was equipped with the visible-light filter, which decreased the lamp's photon flux by half. The suspension of the sample and MB solution was constantly mixed and cooled. After irradiation started, the aliquots of 5 mL were taken every 30 min during the first 150 min of the experiment and then every 60 min to the total of 330 min. The solution was separated from the catalyst at 8000 r.p.m. using air-cooling centrifuge, and concentration was photometrically determined (absorbance measured at 664 nm). Then the solution and the catalyst were returned back to the reactor, and irradiation continued. Photolysis of the MB solution was carried out under the same experimental conditions, but in the absence of a catalyst. The error of MB concentration determination, calculated from the data obtained for replicate runs, did not exceed 7%. The total organic carbon (TOC) was measured using Shimadzu TOC-V CSH Analyzer for the MB solution and the most active sample after 330 min of irradiation.

3. Results and discussion

3.1. EDS and XRD study of SiO_2/TiO_2 particles

When the samples were recovered after hydrothermal treatment, their elemental compositions were analyzed by EDS method. The slight decrease in silica content after synthesis in comparison with the one in the reaction mixture was observed for all of them. The variations between the SiO_2/TiO_2 molar ratios in the reaction mixture and in the solid phase are shown in Table 1. Despite the pH of the reaction mixture after synthesis equaling 3.0 for all the samples, which is explained by decomposition of PTA during heat treatment, the concentration of silica left in the solution is too small to polymerize and it has been removed at washing. Elemental CHNS analysis has proved the absence of sulfur in the prepared silica–titania materials (<0.1 wt%), with the exception for the pure TiO_2 and the 0.1TS samples, where *ca* 1 wt% of sulfur has been detected.

Anatase is known to be the most photocatalytically active polymorph of TiO_2. The increase in its crystallinity and crystallite size could results in lowering the recombination rate, hence provide better photocatalytic activity. That is why the determination of the TiO_2 crystalline phase and its crystal sizes is of great importance. The XRD data (Fig. 1) reveal that all the samples contain only the anatase phase of TiO_2 (ICDD PDF2 99-101-0957), except 0.9TS, where near 2 wt% of rutile phase (ICDD PDF2 99-101-0954) is detected. The as-prepared samples and the ones calcined at 400 °C show no differences in their structural features, crystallite sizes, or any other properties determined by spectroscopic techniques. For the sake of comparison three other silica–titania samples (PTA–SiO_2, GelTS and NH_3PT–SiO_2) have been synthesized, using different combinations of the reagents, and their XRD patterns have been registered (Supplementary Information Fig. S1). From Table 1, where the crystallite sizes estimated by (1 0 1) reflection for the anatase phase using Scherrer equation are presented, it is clear that the sizes of anatase crystals and relative crystallinity are significantly higher in the SiO_2/TiO_2 mixed oxides synthesized by the proposed peroxo route, than they are for the gel subjected to hydrothermal treatment (GelTS), separately prepared titanium peroxo complex and sodium silicate (NH_3PT–SiO_2), or for the sample prepared without any pH adjustment after hydrogel dissolution (PTA–SiO_2). The samples prepared via non-peroxo route were excluded from the further study on the basis of they poorer crystallinity.

Addition of silica has been found to have no significant effect on the changing of *a*-parameter of the TiO_2 unit cell; however, *c*-parameter shows noticeable variations (Table 1). The decrease in the anatase unit cell volume might indicate the formation of Si–O–Ti linkages causing the formation of defects. The lowest value of *c*-parameter is observed for 0.4TS. The variation of this dimension at high silica loadings is not so significant, taking the calculation error into account.

The formation of titania crystallites of larger size, while using the single-source precursor containing titanium peroxo complex and silicic acid, compared to the methods applied to prepare GelTS, PTA–SiO_2 and NH_3PT–SiO_2, can be explained in the following way. The conventional sol–gel or co-precipitation procedures, that routinely serve to synthesize SiO_2/TiO_2 materials, lead to formation of the mixture, which is very homogeneous on the molecular level [25,29]. It is suggested that the incorporation of titania into silica matrix takes place, thus resulting in retardation of TiO_2 crystallization up to high temperatures, and decreased crystallite size of

Table 1
The elemental composition, mean crystallite size, calculated by Scherrer equation, relative crystallinity and the unit cell parameters for anatase in the silica–titania samples (confidence interval of unit cell parameters in brackets).

Sample	Reaction mixture SiO_2/TiO_2 molar ratio	Solid phase SiO_2/TiO_2 molar ratio	Mean crystallite size (nm)	Relative crystallinity	Unit cell parameters (Å)	
					a	*c*
0TS	0	0	10	1	3.785(1)	9.502(1)
0.1TS	0.2	0.1	13	1.12	3.784(4)	9.499(1)
0.4TS	0.5	0.4	24	1.49	3.777(1)	9.428(2)
0.9TS	1.0	0.9	33	1.55	3.782(4)	9.464(3)
1.3TS	1.4	1.3	26	1.37	3.782(1)	9.450(1)
1.6TS	1.8	1.6	16	1.02	3.781(5)	9.459(1)
PTA–SiO_2	1.0	0.9	22	1.24	3.784(5)	9.463(5)
GelTS	1.0	1.0	17	1.26	3.780(1)	9.491(3)
NH_3PT–SiO_2	1.0	0.9	20	1.22	3.781(3)	9.456(2)

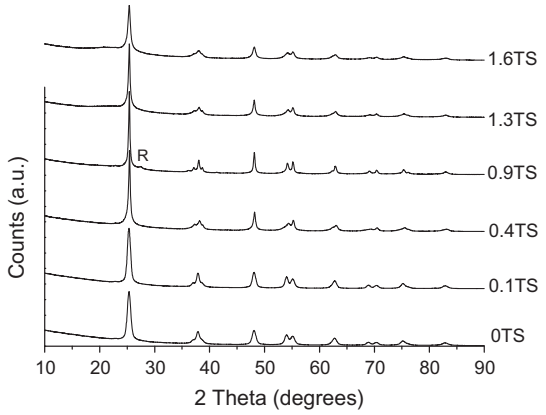

Fig. 1. XRD patterns of the silica–titania samples. *R* – indicates the reflection corresponding to the rutile phase (all the other peaks correspond to anatase).

anatase [25]. However, in the case of the precursor used, one can propose a different interaction mechanism of silica and titania. During the co-precipitation stage Si–O–Ti heterolinkages are formed, but the addition of hydrogen peroxide and ammonia causes their cleavage, and titanium peroxo complex is obtained, while silica stays in oligomeric forms [44]. As Si–O–O–Ti bridges are not likely to appear in this system [48], the degree of titania incorporation in SiO_2 matrix would be less than it is while conventional preparation techniques are applied. When the precursor solution undergoes heating, several processes take place. The rate of hydrogen peroxide and peroxo group decomposition increases drastically, and small seeds of titania are formed. On this stage the state of titania source plays an important part, as it is known that the peroxo method allows decreasing the temperatures of anatase crystallization from the amorphous PTA precursor in comparison with amorphous titania [49]. The initial pH value of 2.0 is determined to be the point when the silica polymerization is low [50], that is why, instead of formation of Si–O–Si network in the whole volume of the reaction mixture, silica species are preferably adsorbed on the surfaces of the formed TiO_2 particles, thus the titania seeds become separated by SiO_2 layer. The rate of diffusion of the dissolved low-concentrated titania species through the silica layer surrounding TiO_2 crystallites is low, and these conditions favor growth of the crystals already existing in the mixture, instead of the formation of new small seeds. The optimal conditions for crystal growth at the given concentrations of silica and titania are reached when the SiO_2/TiO_2 ratio in the solid phase equals 0.9. It is likely that the further increase in silica content favors more rapid polymerization of silica, resulting in the assembling of more rigid SiO_2 network, where diffusion is too hindered to provide the growth of large crystals.

Table 2
XPS surface composition of the mixed oxides and a relative ratio of the silica species obtained from NMR data.

Sample	Si:Ti surface ratio (at%)	$Q^1/Q^2/Q^3/Q^4$ Ratio from ^{29}Si MAS NMR
0TS	0	
0.4TS	1.5:1	1/1.2/7.2/7.3
0.9TS	3.4:1	–/1/4.2/12.3
1.6TS	6.9:1	

3.2. XPS, ^{29}Si MAS NMR, FTIR and DR UV spectroscopic studies

It is obvious now that silica modifies the crystal structure of anatase and controls the sizes of TiO_2 crystals. However, the role of silica species is still unclear, as it is present in the samples in the amorphous state and cannot be established by XRD analysis only. XPS gives some valuable information about the interactions of silica and titania units in the mixed oxides and their surface composition. Silica enriches the surface regions of the silica–titania samples (Table 2), thus making SiO_2 species mainly responsible for the adsorption processes on the silica–titania particles. The shifting of the Ti 2p peak on the XPS spectrum (Fig. 2a) with the increasing silica content indicates the substitution of Si atoms in the SiO_2 network by Ti ones. The displacement of this maximum for the 0.4TS and 0.9TS samples in comparison with 0TS is not significant due to high crystallinity of TiO_2 in the mixed oxides, and as a consequence low degree of Ti incorporation in the silica matrix. At the same time the obvious decrease of binding energy of Ti in 1.6TS correlates with its low crystallinity, as it reflects the incorporation of Ti^{4+} ions in silica matrix. The variations of the binding energy of oxygen are of particular interest in such systems. The band of O ion of Ti–O–Ti and Si–O–Si matrices is observed at 530.5 and 533.5 eV respectively, and the intermediate value of the binding energy is often attributed to the oxygen of Si–O–Ti bonds [24]. It is assumed that the increase of silica content in the mixed oxide gradually shifts the peak of oxygen to higher binding energies. However the peak of oxygen is split in two on the spectra of the mixed oxides with 0.4 and 0.9 SiO_2/TiO_2 molar ratios, indicating on the separation of oxide phases due to high crystallinity of TiO_2 anatase (Fig. 2b). When the SiO_2/TiO_2 molar ratio is increased up to the value of 1.6, the presence of Si–O–Ti linkages becomes evident, as the peak of O 1s is found at 532 eV. From the data obtained by XPS one can conclude that the lowest content of Si–O–Ti bonds is found in the 0.4TS sample.

Although, XPS data say in favor of the separation of the two oxides in the mixed one, more clear understanding of the state of silica is required. The form of the silica species and some information about silicon local structure can be obtained from the solid state ^{29}Si NMR. Two samples with high crystallinity and separation degree of the oxides were investigated using this method. Fig. 3

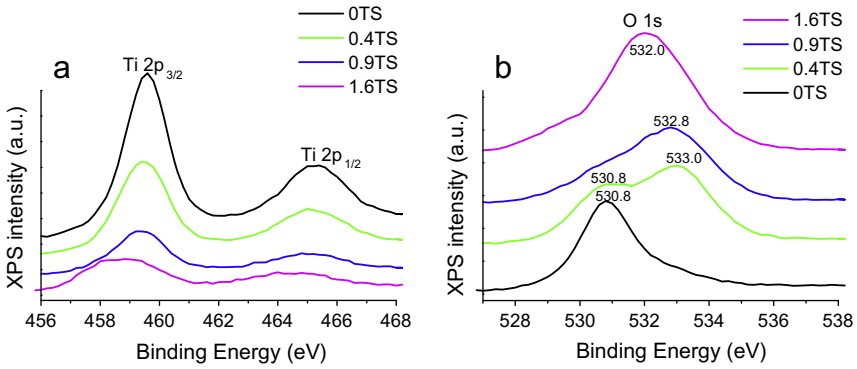

Fig. 2. XPS spectra of Ti 2p (a) and O 1s (b) regions.

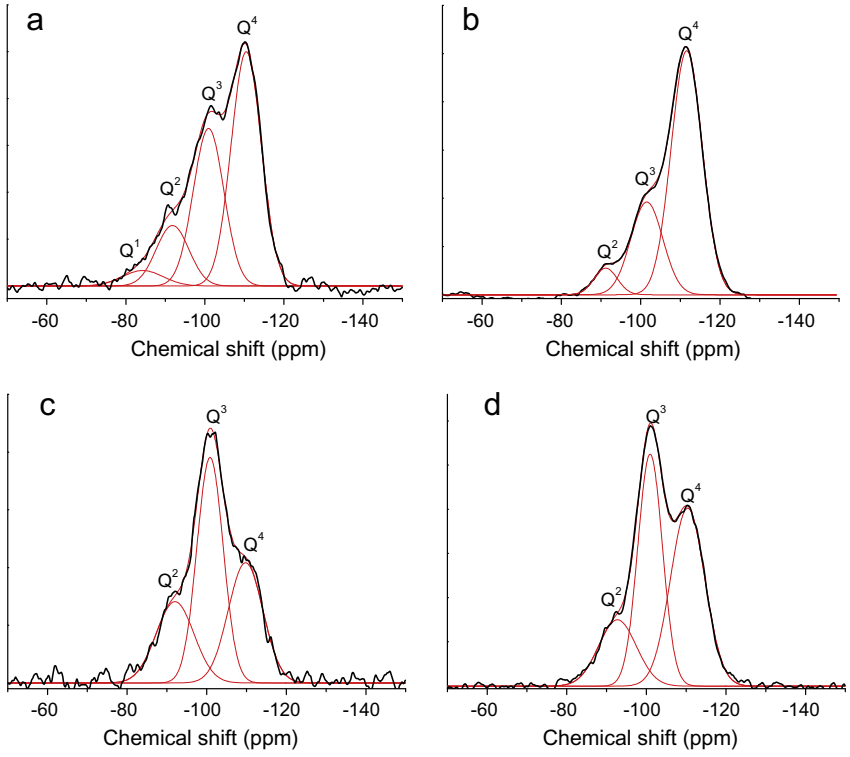

Fig. 3. ^{29}Si MAS and ^{29}Si–^{1}H CPMAS NMR spectra of the (a) 0.4TS, (b) 0.9TS and (c) 0.4TS, (d) 0.9TS samples respectively.

shows the ^{29}Si MAS NMR and ^{29}Si CPMAS NMR spectra of the most crystalline 0.4TS and 0.9TS samples, where the peaks at chemical shifts of approximately 110, 101, and 90 ppm, attributed to the different silica species, are clearly resolved. From Fig. 3a and b it is obvious that the 0.4TS sample contains less amount of highly condensed Q^4 [$Si(SiO)_4$] than its amount in the 0.9TS one (the ratios of the Q^4, Q^3, Q^2 and Q^1 species, calculated from the deconvoluted spectra, are shown in Table 2). The higher content of the low condensed silica can be caused by incorporation of Ti atoms into the SiO_2 matrix, thus forming Si–O–Ti linkages [29], but also by high dispersion of silica particles on titania. Nur observed formation of low condensed units, such as Q^2, after colloidal silica had been dispersed onto preformed titania particles [51]. The influence of Ti incorporation into SiO_2 and OH groups on the chemical shift can be distinguished using ^{29}Si CPMAS NMR. In the case that Ti incorporation gave the main contribution into the formation of Q^2 and Q^3 groups, the enhancement of the intensity of these signals on ^{29}Si CPMAS NMR spectra would be insignificant, but a different picture is seen in Fig. 3c and d. The obvious increase in intensity at 101 and 90 ppm on the spectra of the both samples is clear, while the signal corresponding to Q^1 is not enhanced. This means that the most part of the silicon nuclei is directly bonded to hydroxyl groups, but the silicon of Q^1 species is possibly attributed to the presence of Si–O–Ti. The results of the solid state NMR are in good agreement with those obtained from XPS, as they confirm high degree of separation of silica and titania on the molecular level in the mixed oxides. Moreover, it has been shown that the 0.4TS sample contains higher amount of hydroxyl groups of silica Q^3 and Q^2 species, than the 0.9TS one. However, the presence of Si–O–Ti bonds should not be totally excluded, since they have to be present in some quantities, in order to provide attachment to the surface of titania particles.

The FTIR spectra of the 0TS and 0.1TS samples are almost featureless, only the weak bands corresponding to SO_4^{2-} groups at 1100 cm^{-1} and the broad band centered at 670 cm^{-1}, attributed to vibrations in octahedral TiO_6, are worth mentioning (Fig. 4). The asymmetric stretching vibrations of Si–O–Si bridges at 1070 cm^{-1} in silica become clearly seen and as intense as Ti–O–

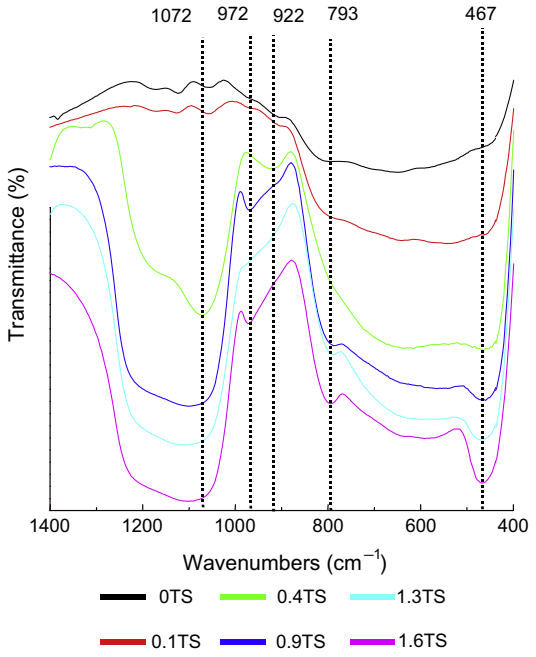

Fig. 4. FTIR spectra of the silica–titania samples.

Ti stretching on the spectrum of the sample with SiO_2/TiO_2 molar ratio equaling 0.4. The peak of Si–O–Si symmetric stretching vibrations near 790–800 cm^{-1}, usually present in the spectra of silica compounds, is not observed on the spectrum of the 0.4TS sample, which can be considered as the indication of the low quantity of highly condensed silica species (Q^4) due to small silica loading and its high dispersion on titania particles. The spectrum of 0.4TS sample shows no presence of this band, while for 0.9TS a peak in this region is observed showing the presence of the condensed SiO_2 network. The bands at 793 cm^{-1} and 467 cm^{-1} increase their intensity and become more prominent with the increase of silica content, and the peak of the asymmetric stretching of Si–O–Si (1100–1070 cm^{-1}) shifts towards higher wavenumbers. It might be suggested that the sample 0.4TS contains lower amount of highly condensed silica, which is in accordance with NMR study. The absorption in the region of 920–980 cm^{-1} corresponds to the joint contribution from silanol groups and Si–O–Ti heterolinkage vibrations, according to numerous reports [25,29,52]. However, the position of this peak is different for 0.4TS and the samples with higher silica content. Considering the XPS results, which evidence the separation of SiO_2 and TiO_2 in the 0.4TS sample and clearly indicate the formation of Si–O–Ti linkages in the 1.6TS sample, one can conclude that the shifting of the peak from 922 cm^{-1} (for the 0.4TS sample) to 972 cm^{-1} (for the 1.6 sample) is assigned to the increasing contribution of Si–O–Ti bond vibration. This feature is more likely to correspond to the higher incorporation degree of Ti atoms into silica network.

The other spectroscopic technique used for the characterization of materials allows calculating band gap energy of semiconductors, which is a feature of high importance for photocatalysts. Expectedly, the band gap energy increases, as the silica content in the SiO_2/TiO_2 samples rises, but this relationship is not linear (S.I. Fig. S2). The widening of the band gap reflects the defectiveness of anatase structure; however the difference of the band gap energy between pure titania and silica–titania is not large. Li and Kim [27] found that the addition of silica caused significant blue shift of the absorption edge, as silica containing samples possessed band gap energy of 3.54 eV, while for pure TiO_2 that value equaled 3.20 eV. In our case not so significant change in the band gap energies can be attributed to high crystallinity of the anatase in the mixed oxides.

3.3. Surface area and porosity measurements

Special attention of the researchers, investigating photocatalytic properties of titania, is attracted to its porous characteristics. Usually, highly crystalline anatase has low surface area [53–55], only seldom exceeding 100 m^2/g [56], which hinders accessibility of active sites for organic molecules. Silica provides TiO_2 with such indispensable properties as mesoporosity and developed surface that result, according to some reports, in enhanced photocatalytic activity [57,58]. We have found the effect of silica addition, when the proposed peroxo route is used, to be different to that is usually observed for the sol–gel materials. The synthesized titania (0TS) shows isotherm type IV with H2 type of the hysteresis loop, typical of mesoporous solids, according to IUPAC classification (Fig. 5a). This sample, having crystallite size of 10 nm, expectedly has high value of surface area (Table 3) and also narrow pore size distribution (S.I. Fig. S3a). Silica at low loadings does not make the surface of the mixed oxide more developed; on the contrary, the surface area of 0.4TS has smaller value in comparison with pure TiO_2 (Table 3). The reduction of the surface area for 0.4TS is undoubtedly related to the increase of TiO_2 crystallite size. The 0.4TS and 0.9TS samples have the isotherm type IV and barely distinguishable hysteresis loops of H1 type (Fig. 5b and c). Pore size distribution analysis has shown the presence of the meso- and macropores (0.9TS sample exhibits two maximums in the pore size distribution, one corresponding to mesopores and another to macropores) in these samples (S.I. Fig. S3b and c), which are likely to be attributed to the interparticle voids. Higher silica content favors developing the surface area of the mixed oxide. The mixed oxide with the highest SiO_2/TiO_2 molar ratio has surface area slightly exceeding the same value obtained for 0TS (Table 3). It is also noticeable that the form of the hysteresis loop is different than it is for previously discussed samples. The H1 type hysteresis loop (Fig. 5d) indicates the formation of mesopores, which are in the range of 10–50 nm (S.I. Fig. S3d).

Silica has a drastic effect on the porosity and surface area of the mixed oxides: it promotes TiO_2 crystallinity and bonds to the anatase crystals forming larger particles, the pores in which are partially blocked by the SiO_2, thus contributing to decrease of the surface area. After the highest degree of silica coverage of TiO_2 particles has been reached, as it is for the 0.4TS sample, SiO_2 starts to form more condensed network, which is confirmed by NMR study, leading to the enhanced surface area of the mixed oxide (0.9TS and 1.6TS) and appearance of mesoporosity at high loadings of SiO_2 (1.6TS).

3.4. SEM and TEM investigations

The evolution of morphology of the prepared mixed oxides is seen in Fig. 6. Pure titania sample (Fig. 6a) is composed of small particles assembled in large shapeless aggregates. The particles of the 0.4TS sample are well separated from each other; they have spherical or slightly elongated forms (Fig. 6b). The most crystalline sample 0.9TS (Fig. 6c) has some similarity to the 0.4TS; however, it is not so uniform. Further increase in silica content results in formation of the dispersed small grains of the mixed oxide surrounding the larger particles (Fig. 6d). The samples 0.4TS and 0.9TS are represented by the aggregates with the mean size 70–90 nm, composed of small spheres having diameter about 10 nm. This observation is inconsistent with the XRD data, as it has been determined that the crystalline sizes of TiO_2 in these samples, calculated by (101) reflection, equal 24 and 33 nm, respectively. Such disagreement forces us to conclude that these particles are titania

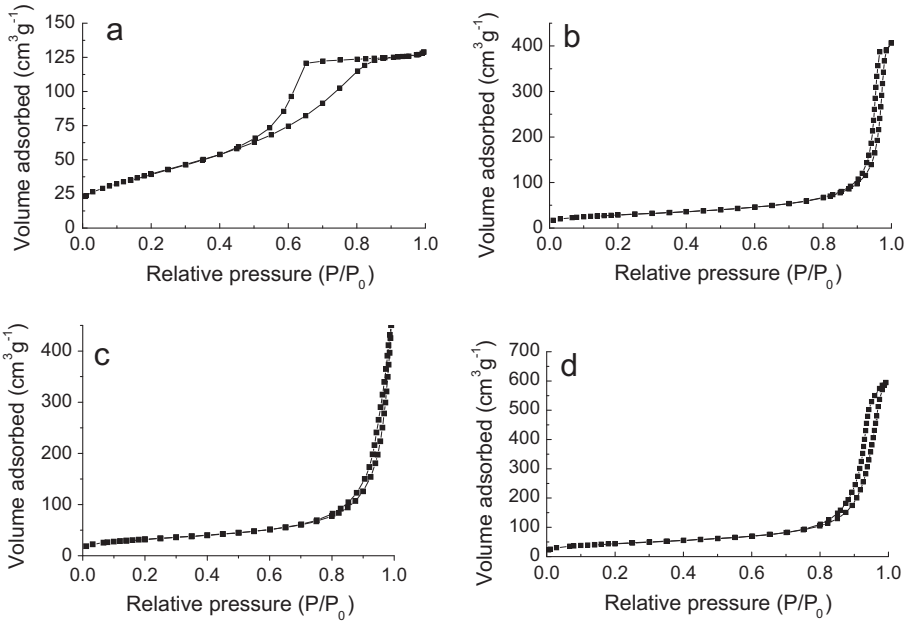

Fig. 5. N_2 adsorption–desorption isotherms of the samples (a) 0TS, (b) 0.4TS, (c) 0.9TS, and (d) 1.6TS.

Table 3
The results of N_2 physisorption experiment.

Sample	BET surface area (m^2/g)
0TS	147
0.4TS	101
0.9TS	113
1.6TS	156

crystals covered by the small silica spheres polymerized on their surfaces.

TEM observations are in good agreement with the crystallite size calculated for pure titania on the basis of XRD data (S.I. Fig. S4). The sample is composed of small crystals of 10–15 nm assembled in large aggregates.

The TEM-images of the 0.4TS sample clearly show its monodispersity and uniformity of particle shapes (Fig. 7a). It can be seen that each particle is composed of the anatase single-crystal covered with amorphous silica particles (Fig. 7b). The elemental analysis from selected area of the particles, made by EDS technique (S.I. Fig. S5), confirms the presence of silica distributed on the surface of titania crystals. The results of elemental analysis made by TEM-EDS technique from the single particles are similar to those obtained for the whole sample; they are presented in Table 1. The titania crystals are elongated along [004], it is seen from the Fig. 7b, and the aspect ratio of the crystal sizes along [004] and

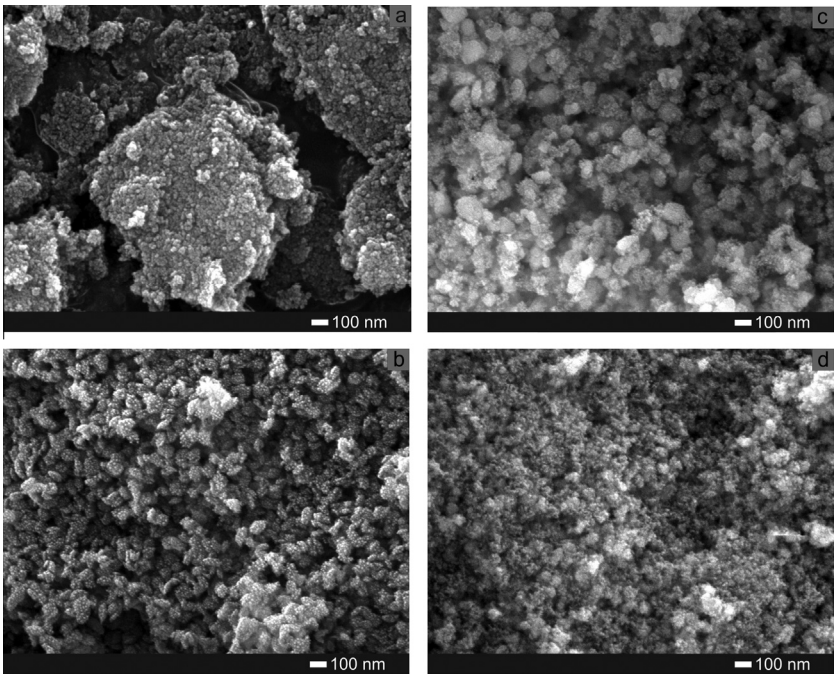

Fig. 6. SEM images of the samples (a) 0TS, (b) 0.4TS, (c) 0.9TS, and (d) 1.6TS.

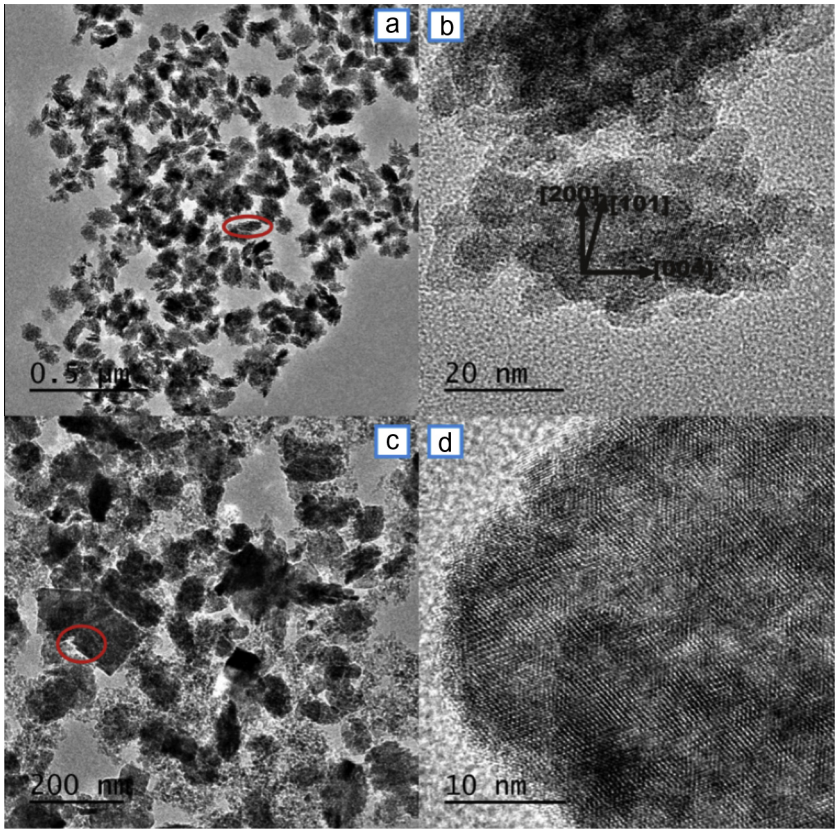

Fig. 7. TEM-images of the 0.4TS sample: (a) a general image of the sample, (b) high resolution micrograph; and the 0.9TS sample: (c) a general image of the sample, (d) high resolution micrograph.

[101] directions is estimated to be equal to 2.2. These changes in morphology of this sample are likely to be responsible for the significant difference of the unit cell parameter (Table 1), as the effect of silica incorporation seems to be less probable in a view of the XPS results.

The greater amount of silica in the mixed oxide samples has resulted in larger crystallites of TiO_2, and has also caused separation of pure silica particles from anatase crystals. Titania exists in the form of crystals having various shapes and sizes, each of them is covered with a layer of adsorbed silica particles (S.I. Fig. S6).

Mostly the particles of the 1.6TS sample are the agglomerates of small titania crystallites, where crystalline anatase is embedded in amorphous SiO_2 matrix. They do not possess any definite shape and the material resembles the one usually obtained in the result of conventional sol–gel procedure. However, the presence of large crystals, similar to those observed for 0.9TS sample, is noticeable (S.I. Fig. S7).

Summarizing the results obtained from different characterization techniques, the following formation mechanism of silica–titania particles can be proposed. In absence of silica titania peroxo species condense rapidly with each other and the solid phase is formed, even the appearance of the sol in the acidic medium indicates that they tend to coalesce. This limits the crystal sizes of TiO_2 within 10 nm, thus the material has high surface area, and uniformity of the particles provides unimodal pore-size distribution (S.I. Fig. 3a). The addition of silica results in its adsorption on the titania species, thus decreasing the rate of their condensation and preventing coalescence. This slows down the crystallization process. It is also important to mention that the Si–O–Ti linkages are cleaved by addition of hydrogen peroxide and PTA and silicic acid present in the reaction mixture separately [44]. These two important features provide slower crystal growth, where the diffusion of dissolved titania species towards formed seeds is controlled by the layer of silica particles formed on their surfaces. At this stage of synthesis the low pH value plays an important part, as silica has low polymerization rate at these conditions [50], so it does not form rigid network around TiO_2 seeds. Indeed, silica in this material is not in the highly condensed state that is evidenced from NMR study. Silica particles cover the titania crystals with a thin amorphous layer having high concentration of hydroxyl groups in the vicinity of the photocatalytically active TiO_2.

It is reasonable that the ability of TiO_2 crystals to accommodate silica species on their surface is limited. When the SiO_2/TiO_2 ratio reaches 0.9, the presence of highly condensed silica becomes obvious from NMR data. We attribute the increase in crystallinity in this sample to the slower rate of condensation of titania species and slower diffusion of dissolved species towards the formed seeds through the silica layer. At this point the mechanism of formation of silica–titania particles changes. In the 1.6TS sample the polymerization of SiO_2 goes faster due to its higher concentration in the reaction mixture, so the mixture of small and large crystallites of TiO_2 embedded in the amorphous SiO_2 is formed. The incorporation of Ti atoms into silica network reaches the highest degree for all investigated samples, which suppresses TiO_2 crystallinity.

3.5. Photocatalytic test

The photocatalytic properties of the prepared mixed oxides are found to be enhanced in comparison with pure titania synthesized under the same conditions and Degussa P25. In Fig. 8a one can see the general trend of MB photodegradation on the titania and silica–titania catalysts. It is noticeable that the 0.4TS and 1.6TS samples have the highest adsorption capacity for MB due to the thin layer of hydroxyl-rich SiO_2 in one case and the presence of Ti–O–Si linkages causing more amorphous character of the oxide in the other (Table 4). The increased crystallinity and the presence of high

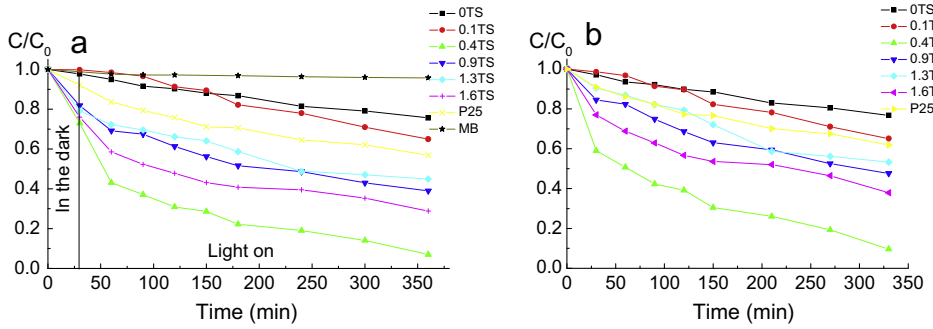

Fig. 8. Photocatalytic decomposition of MB solution on the titania and silica–titania materials (a) showing the values of adsorption of MB on the samples; (b) excluding adsorption stage.

Table 4
First-order kinetic constant (min^{-1}) of MB degradation and adsorption capacity for MB of the pure titania and silica–titania samples.

Sample	0TS	0.1TS	0.4TS	0.9TS	1.3TS	1.6TS	Degussa P25
k_1 (ks^{-1} L g TiO_2^{-1})	0.031	0.043	0.288	0.130	0.104	0.200	0.053
Adsorption (mmol(MB) g^{-1})	1	1	18	11	15	17	5

amount of highly condensed silica species (Q^4) reduce the adsorption capacity of the 0.9TS sample.

The clearer picture of photodecomposition process may be obtained from Fig. 8b, where the adsorption stage is excluded, and the concentration of MB left in the solution after adsorption is taken as C_0. The 0.4TS sample shows activity, which is superior compared with other catalysts. It adsorbs and decomposes more than 90% of MB (S.I. Fig. S8), and, according to TOC determination, 60% of carbon is removed from the solution after adsorption and photocatalysis. In order to discuss the effect of various material properties on the catalyst performance, reaction curves have been fit to a pseudo-first order reaction model (S.I. Fig. S9), the kinetic constant for each material is reported in Table 3. Other kinetic models, such as zero-th order, second order or Langmuir–Hinshelwood models have also been tested, but these models do not provide good fit of the experimental results.

As it has been described earlier, usually the enhanced photocatalytic activity of TiO_2 in mixed silica–titania oxides is attributed to its improved surface area and mesoporosity that silica brings to the binary system, or to the small crystal size of titania. However, it is clear for us that the influence that the porous structure has on the SiO_2/TiO_2 activity is negligible. Crystallinity of the active phase has greater influence on the MB decomposition rate. As the anatase crystal size and its relative crystallinity increase, the decomposition rate increases drastically, this is clearly seen for the 0.4TS, 0.9TS and 1.3TS samples. However, it cannot be the determinative parameter, as there is no correlation between activity and crystallinity. This leads to the consideration of another important factor, adsorption mechanism. The most photocatalytically active 0.4TS sample has the highest adsorption capacity for MB, which is not related to surface area or high silica content, but this value only slightly exceeds the one for the 1.6TS sample, so it clearly cannot be the explanation for the 0.4TS superior performance. The adsorption process and interaction of TiO_2 anatase with the target molecules in the 0.4TS and other silica-rich samples are not similar. It is proved by NMR and TEM analyses that silica in the 0.4TS sample is not in the highly condensed state and it uniformly covers titania crystals. Also it might be suggested that adsorption of organic molecules on the thin layer of amorphous silica is preferred, as it provides the immobilization of target molecules near the photocatalytically active TiO_2. Thus, MB is immobilized on the hydroxyl groups in the vicinity of highly crystalline anatase, while in the samples with high silica loadings it is adsorbed on the silanol groups of the highly condensed SiO_2 network separated from TiO_2 crystals, which could not favor the transfer of the oxidants from anatase surface to MB.

It is difficult to define the property that determines the photocatalytic activity of silica–titania materials to the greater extent, since no direct correlations were found (S.I. Fig. S10), but it is obvious that the presence of thin silica layer rich in hydroxyls, high crystallinity of anatase and the ability to adsorb methylene blue are among the most important.

4. Conclusions

In the present study we have proposed a new completely inorganic method of preparation of the silica–titania photocatalysts, using titanium peroxo complex and silicic acid as the single-source precursor. We have found that in contrast to conventional alkoxide-based or inorganic sol–gel processes, silica does not suppress titania crystal growth; on the contrary, it favors improving TiO_2 crystallinity. It has been proposed that this is caused by the low degree of Ti incorporation in SiO_2 in the precursor and by the adsorption of silica species on the titania seeds separating them from each other, thus controlling diffusion and saturation conditions in the reaction mixture. The sample with the SiO_2/TiO_2 ratio of 0.9 has the highest relative crystallinity and the largest titania crystallite size. The sample with SiO_2/TiO_2 molar ratio equaling 0.4 is found to be the most uniform in the sense of particle size distribution, and also it has shown the superior performance in photocatalytic decomposition of methylene blue. We attribute the enhanced photocatalytic activity of the synthesized mixed oxides compared to pure TiO_2 to the adsorption of methylene blue on the thin silica layer rich in hydroxyls in the vicinity of highly crystalline anatase TiO_2.

Acknowledgments

South Ural State University acknowledges financial support of The Ministry of Education and Science of the Russian Federation Grant No 16.2674.2014/K. The study is also carried out within grants of Spanish MINECO (MAT2013-40950-R; CTQ2011-29272-C04-02). Marina Ilkaeva thanks the government of the Principality

of Asturias for a Ph.D. fellowship (Severo Ochoa programm) BP 14-029.

Appendix A. Supplementary material

The XRD patterns of the PTA–SiO_2, GelTS and NH_3PT–SiO_2 samples, pore size distribution analysis, the results of band gap energy determination and TEM-EDS analysis of the silica–titania particles. Supplementary data associated with this article can be found, in the online version, at http://dx.doi.org/10.1016/j.jcis.2014.12.044.

References

[1] G. Liu, L. Wang, H.G. Yang, H-M. Cheng, G.Q. (Max) Lu, J. Mater. Chem. 20 (2010) 831–843.
[2] H. Chen, C.E. Nanayakkara, V.H. Grassian, Chem. Rev. 112 (2012) 5919–5948.
[3] S. Liu, J. Yu, M. Jaroniec, Chem. Mater. 23 (2011) 4085–4093.
[4] A.A. Ismail, D.W. Bahnemann, J. Mater. Chem. 21 (2011) 11686–11707.
[5] R. Daghrir, P. Drogui, D. Robert, Ind. Eng. Chem. Res. 52 (2013) 3581–3599.
[6] D.J. Stacchiola, S.D. Senanayake, P. Liu, J.R. Rodriguez, Chem. Rev. 113 (2013) 4373–4390.
[7] W.Y. Teoh, J.A. Scott, R. Amal, J. Phys. Chem. Lett. 3 (2012) 629–639.
[8] M. Pagliaro, G. Palmisano, R. Ciriminna, V. Loddo, Energy Environ. Sci. 2 (2009) 838–844.
[9] U.G. Akpan, B.H. Hameed, J. Hazard. Mater. 170 (2009) 520–529.
[10] I.A. Konstantinou, T.A. Albanis, Appl. Catal., B: Environ. 49 (2004) 1–14.
[11] Z. Weng, G. Guo, G. Liu, S. Wu, K.W.K. Yeng, P.K. Chu, RSC Adv. 3 (2013) 24758–24775.
[12] A. Kubacka, M. Fernández-García, G. Colon, Chem. Rev. 112 (2012) 1555–1614.
[13] J.-Y. Piquemal, E. Briot, J.-M. Bregeault, Dalton Trans. 42 (2013) 29–45.
[14] M. Kakihana, M. Kobayashi, K. Tomita, V. Petrykin, Bull. Chem. Soc. Jpn. 83 (2010) 1285–1308.
[15] V.G. Kessler, J. Sol–Gel. Sci. Technol. 68 (2013) 464–470.
[16] K. Tomita, V. Petrykin, M. Kobayashi, M. Shiro, M. Yoshimura, M. Kakihana, Angew. Chem. 188 (2006) 2438–2441.
[17] Y. Zhang, L. Wu, Q. Zheng, J. Zhi, J. Phys. Chem. C 112 (2008) 16457–16462.
[18] N. Murakami, Y. Kurihara, T. Tsubota, T. Ohno, J. Phys. Chem. C 113 (2009) 3062–3069.
[19] J.A. Chang, M. Vithal, I.C. Baek, S.I. Seok, J. Solid State Chem. 182 (2009) 749–756.
[20] V.R. De Mendoca, C. Ribeiro, Appl. Catal., B: Environ. 105 (2011) 298–305.
[21] Y. Miao, J. Gao, J. Solid State Chem. 196 (2012) 372–378.
[22] M. Kobayashi, V. Petrykin, K. Tomita, M. Kakihana, J. Cryst. Growth 337 (2011) 30–37.
[23] A. Ennaoui, B.R. Sankapal, V. Skryshevsky, Mch. Lux-Steiner, Cell 90 (2006) 1533–1541.
[24] H.S. Kibombo, R. Peng, S. Rasalingam, R.T. Koodali, Catal. Sci. Technol. 2 (2012) 1737–1766.
[25] H.S. Kibombo, D. Zhao, A. Gonshorowski, S. Budhi, M.D. Koppang, R.T. Koodali, J. Phys. Chem. C 115 (2011) 6126–6135.
[26] Z. Li, B. Hou, Y. Xu, D. Wu, Y. Sun, W. Hu, F. Deng, F. Comparative, J. Solid State Chem. 178 (2005) 1395–1405.
[27] Y. Li, S.-J. Kim, J. Phys. Chem. B 109 (2005) 12309–12315.
[28] W. Dong, Y. Sun, C.W. Lee, W. Hua, X. Lu, Y. Shi, S. Zhang, J. Chen, D.J. Zhao, J. Am. Chem. Soc. 129 (2007) 13894–13904.
[29] R.J. Davis, Z. Liu, Chem. Mater. 9 (1997) 2311–2324.
[30] Y. Ren, Y. Zhang, L. Wu, Langmuir 26 (2010) 11391–11396.
[31] X. Li, J. He, ACS Appl. Mater. Interfaces 5 (2013) 5282–5290.
[32] Z.Y. Wu, Y.F. Tao, Z. Lin, L. Liu, X.X. Fan, Y. Wang, J. Phys. Chem. C 113 (2009) 20335–20348.
[33] B. Mahltig, E. Gutmann, D.C. Meyer, Mater. Chem. Phys. 127 (2011) 285–291.
[34] M. Andrianainarivelo, R. Corriu, D. Leclercq, P.H. Mutin, A. Vioux, J. Mater. Chem. 6 (1996) 1665–1671.
[35] G. Liu, Y. Liu, G. Yang, S. Li, Y. Zu, W. Zhang, M. Jia, J. Phys. Chem. C 113 (2009) 9345–9351.
[36] A. Budnyk, A. Damin, S. Bordgia, A. Zecchina, J. Phys. Chem. C 116 (2012) 10064–10072.
[37] M. Hirano, K. Ota, H. Iwata, Chem. Mater. 16 (2004) 3725–3732.
[38] X. Chen, S. Shen, L. Guo, S.S. Mao, Chem. Rev. 110 (2010) 6503–6570.
[39] X. Wang, L. Cao, D. Chen, R.A. Caruso, ACS Appl. Mater. Interfaces 5 (2013) 10926–10932.
[40] F. Amano, A. Yamakata, K. Nogami, M. Osawa, B. Ohtani, J. Am. Chem. Soc. 130 (2008) 17650–17651.
[41] M. Anpo, T. Shima, S. Kodama, Y. Kubokawa, J. Phys. Chem. 91 (1987) 4305–4310.
[42] N. Xu, Z. Shi, Y. Fan, J. Dong, J. Shi, M.Z-C. Hu, Ind. Eng. Chem. Res. 38 (1999) 373–379.
[43] I.V. Krivtsov, M.V. Ilkaeva, V.D. Samokhina, V.V. Avdin, S.A. Khainakov, D.A. Uchaev, J.R. Garcia, J. Sol–Gel. Sci. Technol. 67 (2013) 665–669.
[44] M. Ilkaeva, I. Krivtsov, V. Avdin, S. Khainakov, J.R. Garcia, Colloids Surf., A. – Physicochem. Eng. Asp. 456 (2014) 120–128.
[45] A.C. Larson, R.B. Von Dreele, General Structure Analysis System (GSAS), Los Alamos National Laboratory Report LAUR, 1994, pp. 86–748.
[46] X. Wang, T. Dornom, M. Blackford, R.A. Caruso, J. Mater. Chem. 22 (2012) 11701–11710.
[47] J. Yu, F. Fan, K. Lv, Nanoscale 2 (2010) 2144–2149.
[48] W. Lin, H. Frei, J. Am. Chem. Soc. 124 (2002) 9292–9298.
[49] H. Ichinose, M. Terasaki, H. Katsuki, J. Ceram. Soc. Jpn. 104 (1996) 715–718.
[50] R.K. Iler, The Chemistry of Silica, Wiley & Sons, New York, 1979.
[51] H. Nur, Mater. Sci. Eng., B 133 (2006) 49–54.
[52] D.M. Pickup, G. Mountjoy, G.M. Wallidge, R. Anderson, J.M. Cole, R.J. Newport, M.E. Smith, J. Mater. Chem. 9 (1999) 1299–1305.
[53] W. Li, Y. Bai, C. Liu, Z. Yang, X. Feng, X. Lu, N.K. Van der Laak, K-Y. Chan, Environ. Sci. Technol. 43 (2009) 5423–5428.
[54] S.C. Pillai, P. Periyat, R. George, D.E. McCormack, M.K. Seery, H. Hayden, J. Colreavy, D. Corr, S.J. Hinder, J. Phys. Chem. C 111 (2007) 1605–1611.
[55] P. Periyat, S.C. Pillai, D.E. Mccormack, J. Colreavy, S.J. Hinder, J. Phys. Chem. C 112 (2008) 7644–7652.
[56] P. Wen, H. Itoh, W. Tang, Q. Feng, Langmuir 23 (2007) 11782–11790.
[57] X. Chen, X. Wang, X. Fu, Energy Environ. Sci. 2 (2009) 872–877.
[58] X. Fu, L.A. Clark, Q. Yang, M.A. Anderson, Environ. Sci. Technol. 30 (1996) 647–653.